Stem Cell Reports
Article

ISSCR

OPEN ACCESS

Activating a Reserve Neural Stem Cell Population *In Vitro* Enables Engraftment and Multipotency after Transplantation

Jesse Peterson,[1,2] Brian Lin,[1,2] Camila M. Barrios-Camacho,[1,2] Daniel B. Herrick,[1,2] Eric H. Holbrook,[3] Woochan Jang,[1] Julie H. Coleman,[1,2] and James E. Schwob[1,*]

[1]Department of Developmental, Molecular & Chemical Biology, Tufts University School of Medicine, Boston, MA 02111, USA
[2]Sackler School of Graduate Biomedical Sciences, Tufts University, Boston, MA 02111, USA
[3]Department of Otolaryngology, Massachusetts Eye and Ear Infirmary, Harvard Medical School, Boston, MA 02114, USA
*Correspondence: jim.schwob@tufts.edu
https://doi.org/10.1016/j.stemcr.2019.02.014

SUMMARY

The olfactory epithelium (OE) regenerates after injury via two types of tissue stem cells: active globose cells (GBCs) and dormant horizontal basal cells (HBCs). HBCs are roused to activated status by OE injury when P63 levels fall. However, an in-depth understanding of activation requires a system for culturing them that maintains both their self-renewal and multipotency while preventing spontaneous differentiation. Here, we demonstrate that mouse, rat, and human HBCs can be cultured and passaged as P63+ multipotent cells. HBCs *in vitro* closely resemble HBCs *in vivo* based on immunocytochemical and transcriptomic comparisons. Genetic lineage analysis demonstrates that HBCs in culture arise from both tissue-derived HBCs and multipotent GBCs. Treatment with retinoic acid induces neuronal and non-neuronal differentiation and primes cultured HBCs for transplantation into the lesioned OE. Engrafted HBCs generate all OE cell types, including olfactory sensory neurons, confirming that HBC multipotency and neurocompetency are maintained in culture.

INTRODUCTION

In contrast to the rest of the nervous system, the mammalian olfactory epithelium (OE) retains a lifelong capacity for neurogenesis and robust structural and functional regeneration in response to injury, such that the population of olfactory sensory neurons (OSNs) and all of the non-neuronal cell types are nearly perfectly reconstituted during recovery of the tissue (Monti Graziadei and Graziadei, 1979; Schwob et al., 1995, 2017).

The unique resiliency of the OE is conferred by the persistence of two neurocompetent stem cell populations in the basal compartment of the epithelium: the globose basal cells (GBCs) and the horizontal basal cells (HBCs). GBCs are heterogeneous with respect to molecular phenotype and capacity as progenitors (Schwob et al., 2017). In contrast, HBCs are an ostensibly homogeneous "reserve" population of flat, mitotically quiescent cells that adhere to the basal lamina and resemble basal cells of other stratified epithelia morphologically, histologically, and molecularly (Holbrook et al., 1995). Here as elsewhere, the two types of OE stem cells are distinguished by their contextual requirements for stem cell function. In healthy OE, GBCs repopulate cells lost to routine turnover, especially the OSNs. In contrast, HBCs are dormant and rarely differentiate in uninjured OE. However, following acute epithelial injury, HBCs release from the basal lamina, become proliferative, and differentiate into GBCs, which replace cells that were lost due to lesion—an array of behaviors collectively termed HBC activation (Leung et al., 2007).

Recent studies have demonstrated that the transcription factor ΔN-P63α, the predominant isoform of P63 in the OE, is expressed exclusively in HBCs and functions as the "master control switch" of their dormancy and activation (Fletcher et al., 2017, 2011; Packard et al., 2011; Schnittke et al., 2015). For activation to occur, it is both necessary and sufficient for P63 levels to decline (Fletcher et al., 2011; Schnittke et al., 2015). A conditional knockout approach has identified some aspects of p63 regulation. For example, Notch1 signaling in HBCs maintains *p63* expression (Herrick et al., 2017). However, further characterization of P63 regulation in HBCs is hampered by the glacial pace of *in vivo* identification and manipulation of molecular candidates.

Attempts to culture stem and progenitor cells from the OE have been successful in offering some insights into the regulation of GBCs (Beites et al., 2005; Goldstein et al., 2015; Jang et al., 2008; Krolewski et al., 2011; Murdoch and Roskams, 2007). Attempts to culture HBCs from the adult OE have been considerably less successful. As a quiescent population, these cells do not proliferate or expand to an appreciable extent *in vivo*, and cultures are prone to overgrowth by a fibroblast-like spindle cell of unknown origin (Jang et al., 2008). Nonetheless, HBCs offer several conceptual advantages over GBCs for cell replacement therapy. The heterogeneity of potencies in GBCs can result in uncontrolled differentiation in culture and complicates their expansion and cryopreservation, two attributes that are requisite for basic research and critical for therapeutic applications. In contrast, that P63 serves as a master switch for releasing the dormant multipotency of

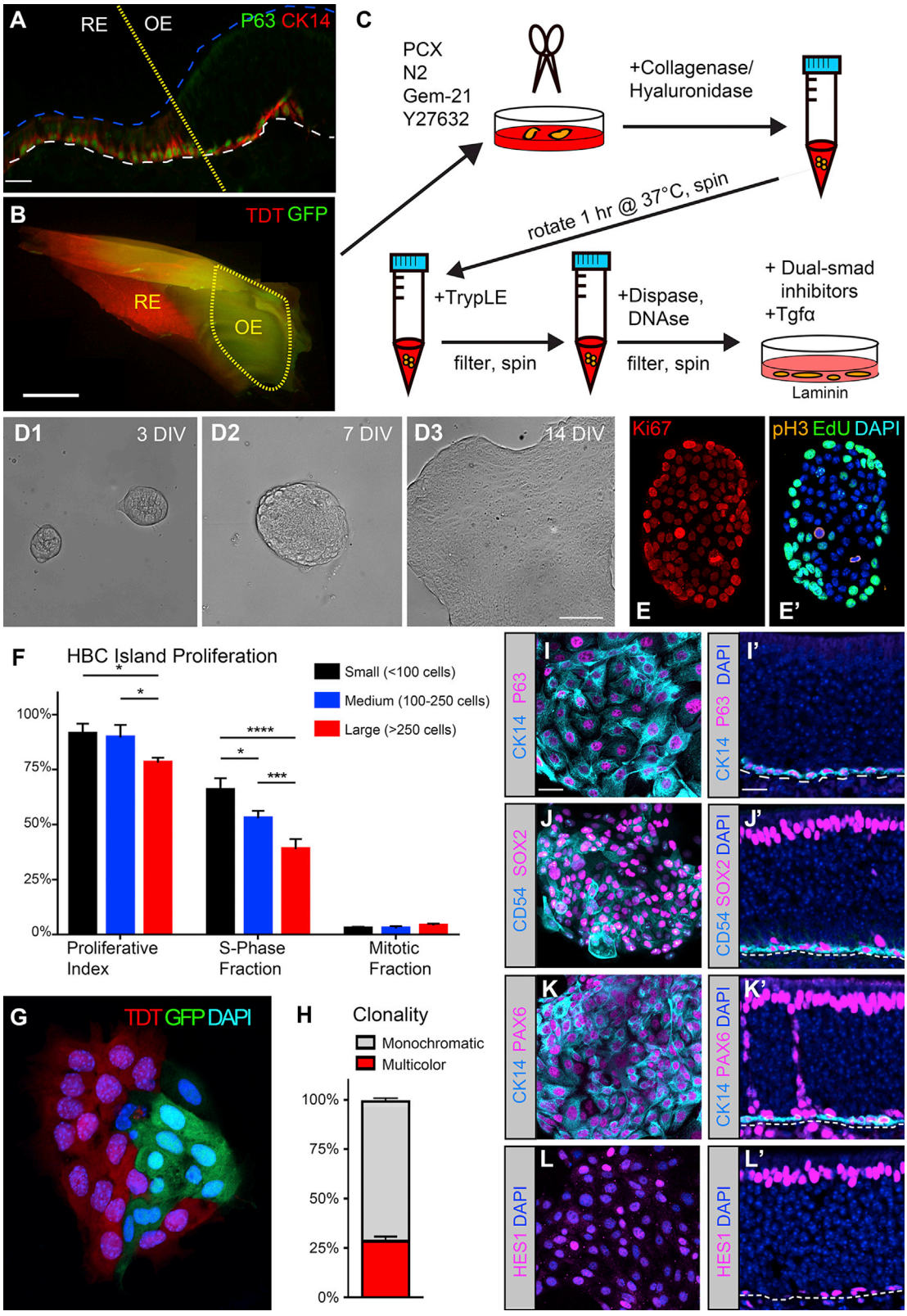

(legend on next page)

HBCs will afford precise control over HBC differentiation *in vitro*.

Therefore, we have developed a robust culture model that allows for HBC expansion while maintaining inherent neurocompetency and multipotency both *in vitro* and *in vivo*.

RESULTS

A Modified Respiratory Culture System Supports Horizontal Basal Cell Growth

Based on the similarities between the CK14+/P63+ HBCs of the OE and the CK14+/P63+ basal cells of the neighboring respiratory epithelium (RE) (Figure 1A), we tested whether bronchial epithelial growth medium (BEGM) or the fully defined Pneumacult-Ex (PCX) alternative could be modified to support HBC growth. OE was isolated from the posterodorsal septum of adult mice (Figure 1B) and enzymatically dissociated, and the cells were plated in a base medium of either BEGM or PCX (Figure 1C). The base medium was amended by the addition of neurobasal supplements, Y27632, dual-SMAD inhibitors, and transforming growth factor α (TGF-α) (Farbman and Buchholz, 1996; Farbman and Ezeh, 2000; Getchell et al., 2000). The best substrate for epithelial cell growth and suppression of fibroblast-like spindle cells was laminin compared with collagen I, collagen IV, fibronectin, Matrigel, and poly-D-lysine.

After 3 days in culture, compact clusters of cells were observed that progressed to form flat epithelial sheets (Figures 1D1–1D3). Cell proliferation was concentrated at the periphery of the clusters (Figures 1E and 1E′), and the fraction of dividing cells decreased as the clusters grew in size (Figure 1F). We assessed clonality by mixing tissue from two strains of mice expressing either constitutive eGFP and TdTOMATO (TDT). The incidence of the mixed GFP-TDT-containing islands (Figures 1G and 1H) suggests that the cultures are not exclusively clonal.

After four passages, we compared the molecular phenotype of the *in vitro* HBCs with *in vivo* HBCs. The islands expressed the HBC markers CK14, CD54, SOX2, PAX6, and HES1 (cf. Figures 1I and 1L versus 1I′and 1L′). K5-CreER^{T2}-driven expression of TDT was also limited to cells in the islands (Figures S1A and S1B). Furthermore, they did not express markers of other epithelial cell types. While Sox2 is common to both HBCs and GBCs, HBCs in culture did not express the GBC markers ASCL1 (also known as Mash1) or NEUROD1 (Figures 2A–2B′), nor did they express the neuronal proteins βIII-TUBULIN (recognized by Tuj1) or OMP, which, taken together, span all of the OSN maturation stages in the OE (Figures 2C–2D′). The putative HBCs lacked CK18, normally found in Sus cells and Bowman's ducts/glands (D/G), although they did express SOX9, which strongly stains Sus/D/G cells but is expressed at low levels in dormant HBCs *in vivo* (Figures 2E and 2E′) and at higher levels after injury. Finally, the cells did not label with the microvillar (MV) marker TRPM5 (Figures 2F and 2F′). Heterogeneity in culture decreased as a function of passage number (Figure 2G), suggesting that the culture conditions are optimal for CK14+/P63+ cells. Analytical fluorescence-activated cell sorting (FACS) assessment confirmed that adherent cultures were enriched in P63+

Figure 1. Isolation and Growth Pattern of HBCs *In Vitro*

(A) CK14+/p63+ HBCs of the OE form a continuous, uninterrupted monolayer with a transition to respiratory basal cells at the boundary between the OE and the RE.

(B) Region of mouse nasal septum harvested for culture is delimited by the dashed line; scale bar, 2 mm. Homogeneity of the dissociated region demonstrated in a transgenic *ΔOMP-eGFP;R26R-TdTomato* mouse expressing *OMP*-driven GFP as well as *Rosa26*-driven TDTOMATO (TDT).

(C) Schematic illustrating the dissociation protocol.

(D1–D3) Epithelial island expansion as a function of time *in vitro*; scale bar in (D3) represents 40 μm and also applies to the other two images.

(E and E′) Representative HBC island demonstrating a high rate of proliferation.

(F) Quantification of cell proliferation based on island size; n = 3 biological replicates. Proliferative index equals Ki67+/total cell number, S-phase fraction equals EdU+/Ki67+, and mitotic fraction equals pH3+/Ki67+ (mean ± SEM). Statistical significance tested by two-way ANOVA with Tukey's multiple comparison test; statistical approach described fully in the Experimental Procedures section. *$p < 0.05$, ***$p < 0.001$, ****$p < 0.0001$.

(G) Example of the non-clonal derivation of an HBC island in cultures grown from a mixture of cells from separate constitutive GFP- and constitutive TdTomato-expressing mice.

(H) Counts of islands composed of red-only/green-only ("monochromatic") or mix of red and green cells ("multicolor"); n = 30 islands from a pooled sample of three septum dissociations (mean ± SEM).

(I–L) Cells in the islands express a number of markers that stain HBCs *in vivo*: (I and I′) the HBC-specific cytokeratin (CK14) and the HBC-marking transcription factor P63; (J and J′) HBC-specific marker CD54 and HBC-marking transcription factor SOX2; (K and K′) CK14 and PAX6; (L, L1) HES1. Dashed lines mark the basal laminae. Scale bars in (I) and (I′) represent 15 μm and apply to all of their respective *in vitro* and *in vivo* panels.

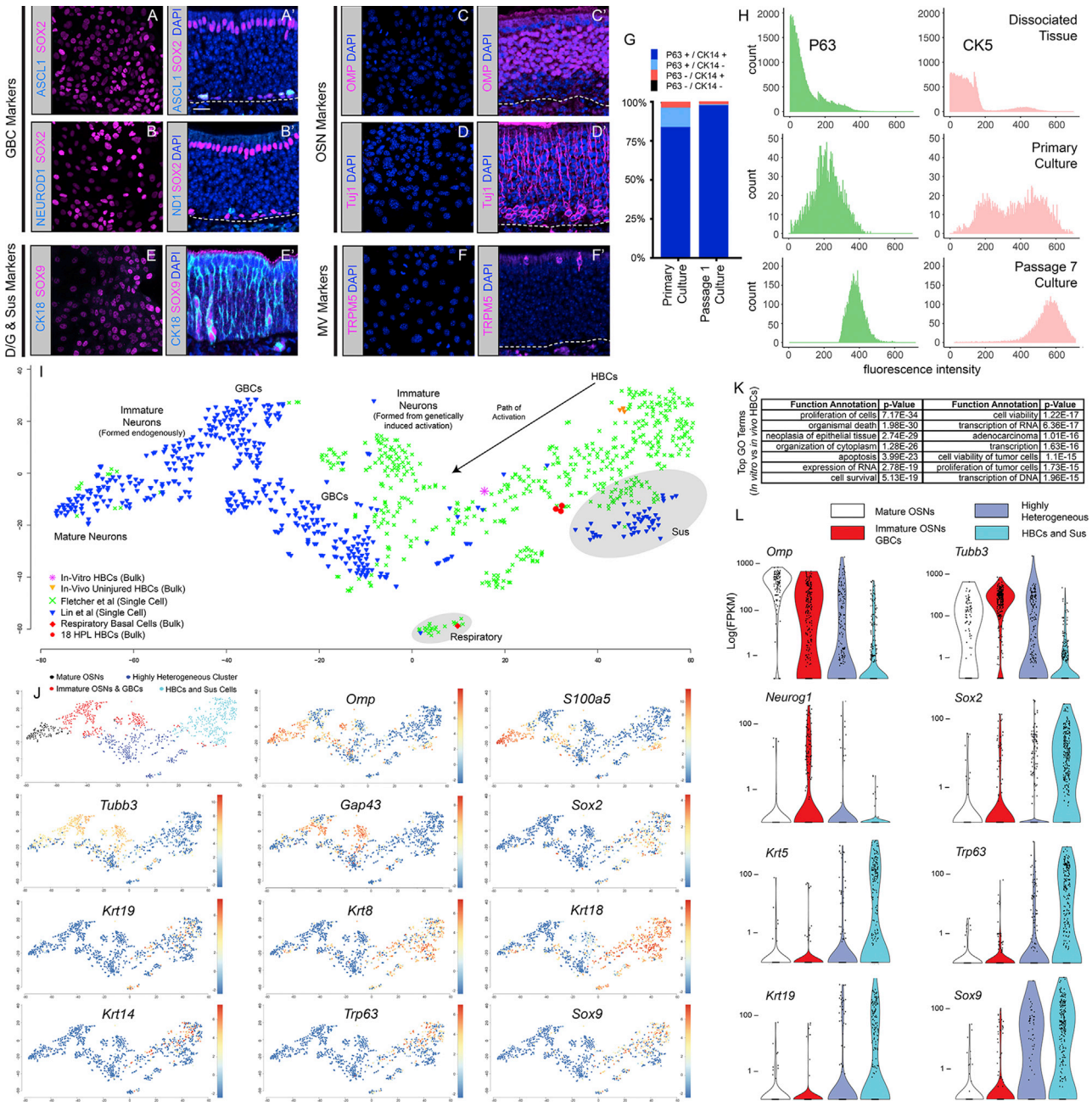

Figure 2. HBCs *In Vitro* Recapitulate the Molecular Profile of HBCs *In Vivo*

(A–F′) Fourth passage HBCs *in vitro* do not express detectable levels of proteins present in GBCs (A–B′), OSNs (C–D′), Sus cells (E and E′), or microvillar cells (F and F′). (In B′, ND1 signifies NeuroD1). SOX9 is expressed by HBCs *in vitro*, and *Sox9* mRNA is found at low levels in HBCs *in vivo*. Strong SOX9 staining is characteristic of D/G cells *in vivo*. However, the absence of CK18 from the HBCs *in vitro* differentiates them from D/G cells *in vivo*. Dashed lines indicate basal laminae. Scale bar in (A′) represents 15 μm and applies to all images.

(G) Under these conditions cultures become homogeneous with respect to phenotype quickly. Quantification of CK14/P63 expression before and after the first passage from low power fields containing a minimum of 300 cells/field.

(H) The cultures become more homogeneous with respect to molecular phenotype over time and passagings. FACS analysis following intracellular immunocytochemistry for P63 and the specific HBC marker CK5 in acutely dissociated tissue, primary culture, and passage 7 culture. Counts exceed 750K, 5K, and 12K cells, respectively.

(I) t-SNE dimension reduction of combined bulk RNA-seq transcriptomes of *in vivo* HBCs from the unlesioned OE, *in vivo* HBCs harvested 18 h post-MeBr lesion (18 HPL), *in vivo* respiratory basal cells, and *in vitro* passage 3 cultured HBCs, single-cell RNA-seq transcriptomes of

(legend continued on next page)

and CK5+ cells compared with whole dissociated OE and that this enrichment had substantially increased by passage 7 (Figure 2H).

After confirming the fidelity of this murine culture model, we found that the same protocol supported the growth of CK14+/P63+/SOX2+ cells dissociated from adult human and adult rat OE (Figure 3), although differences in cell size and morphology are apparent (cf. Figures 3 versus 1).

All subsequent data were taken from cells cultured in proprietary PCX medium unless otherwise specified; however, modified BEGM produced similar results (Figures S1C1–S1C3).

Proliferative HBC Cultures Are Transcriptionally Equivalent to *In Vivo* HBCs

To assess further the degree of similarity between our cultures and other cell types found in OE, we performed RNA-sequencing (RNA-seq) analysis on post-passage cells and compared the culture transcriptome with published RNA-seq data. The published datasets derive from cells harvested from the epithelium directly: bulk-level, FACS-purified HBCs (Herrick et al., 2017), and single-cell RNA-seq of HBCs (Fletcher et al., 2017). Together the transcriptomic data provide a roadmap demonstrating the steps from quiescent stem cell activation, through the progenitor state, to the final mature cell types of the tissue. *In vitro* HBCs clustered closely with *in vivo* HBCs and not with respiratory basal cells (Figure 2I). Cultured HBCs are found at an intermediate stage between dormant and fully activated HBCs. Notably, gene ontology analysis confirmed that the greatest difference between dormant HBCs *in vivo* and the cultured cells can be attributed to the higher rate of proliferation *in vitro* (Figure 2K).

HBCs in Culture Are Derived from *In Vivo* HBCs and ASCL1+ GBCs

The emergent homogeneity of HBC cultures was striking given the diversity of cell types present in the harvested tissue and may be driven by SMAD inhibition (Mou et al., 2016). We assayed which *in vivo* cell type(s) give rise to the HBCs *in vitro*. In the embryo, HBCs emerge perinatally from olfactory placode-like cells that initiate P63 expression (Packard et al., 2011). Moreover, GBCs can regenerate HBCs during epithelial recovery from injury (Goldstein et al., 1998; Lin et al., 2017). To define the origin of the HBCs *in vitro*, we initiated genetic lineage tracing by HBCs and GBCs *in vivo* prior to culture (Figure 4A). The extent and specificity of tamoxifen (Tam)-induced recombination was confirmed by histological examination of a turbinate from each mouse.

Tam-treated *K5-CreER^{T2};fl(STOP)TdT* mice, which label HBCs and their progeny, gave rise to about 75% of the HBCs in the cultures (Figures 4B–4C′). Tam-treated *Ascl1-CreER^{T2};fl(STOP)TdT* mice, which label ASCL1+ GBCs and their neuronal progeny in the undamaged OE, gave rise to about 25% of the total HBCs *in vitro* and were phenotypically equivalent to the HBC-derived ones (Figures 4D–4E′ and 4H). Thus, harvested HBCs and Ascl1+ GBCs generate the majority of the HBCs in culture (Figure 4H). In contrast, Tam-treated *Neurog1-CreER^{T2};fl(STOP)TdT* mice, which label GBCs that are downstream of ASCL1+ in the neurogenic hierarchy (Schwob et al., 2017), did not give rise to HBCs when harvested from uninjured OE (Figures 4F–4G′). However, *Neurog1* mice that were Tam treated and lesioned by injection of methimazole immediately prior to dissociation (Figure 4I) did generate rare TDT + HBCs in culture (<1%) (Figures 4H–4J′); the broadening of the potency of NEUROG1+ GBCs following injury matches our recent findings *in vivo* (Lin et al., 2017).

HBCs in Culture Differentiate after Excision of *p63* or in Response to Retinoic Acid

We tested whether HBCs in culture retain their native multipotency and whether P63 continues to regulate HBC activation/quiescence. HBC cultures were established from *K5-CreER^{T2};fl(STOP)-TdT;p63$^{fl/fl}$* mice, which provide a Tam-inducible, *p63* knockout model (Figure 5A). (Z)-4-Hydroxytamoxifen was added after 10 days *in vitro* and then harvested 4 days later to determine the effect of P63 loss (Figure 5B). Recombination efficiency was low (<5%), but TDT+/P63− cells expressed markers of differentiating

whole dissociated OE, which serve as a bioinformatic reference for comparison (Lin et al., 2017), and single-cell RNA-seq transcriptomes of HBCs before and after activation by excision of P63 (Fletcher et al., 2017). The bulk RNA-seq data serve as reference points for well-defined population-level transcriptomes. The wild-type dissociated OE dataset places the t-SNE plot in the context of the whole tissue. The HBC single-cell dataset serves to expand the differences between truly quiescent HBCs and activated HBCs (Fletcher et al., 2017). With the high resolution of the combined dataset, respiratory basal cells clearly segregate away from both *in vivo* and *in vitro* cultured HBCs.

(J) t-SNE plots with overlaid expression levels of well-characterized marker genes in the OE providing both the basis of cell identity, as well as the non-discrete, transitory nature of each cell population.

(K) Gene ontology analysis on overrepresented, differentially expressed genes between HBCs *in vitro* and uninjured HBCs *in vivo*. Overrepresented genes largely fall into pathways concerned with cell proliferation.

(L) Violin plots of the four major populations depicted in (J) to better demonstrate the expression levels and heterogeneity of various well-characterized markers within the OE.

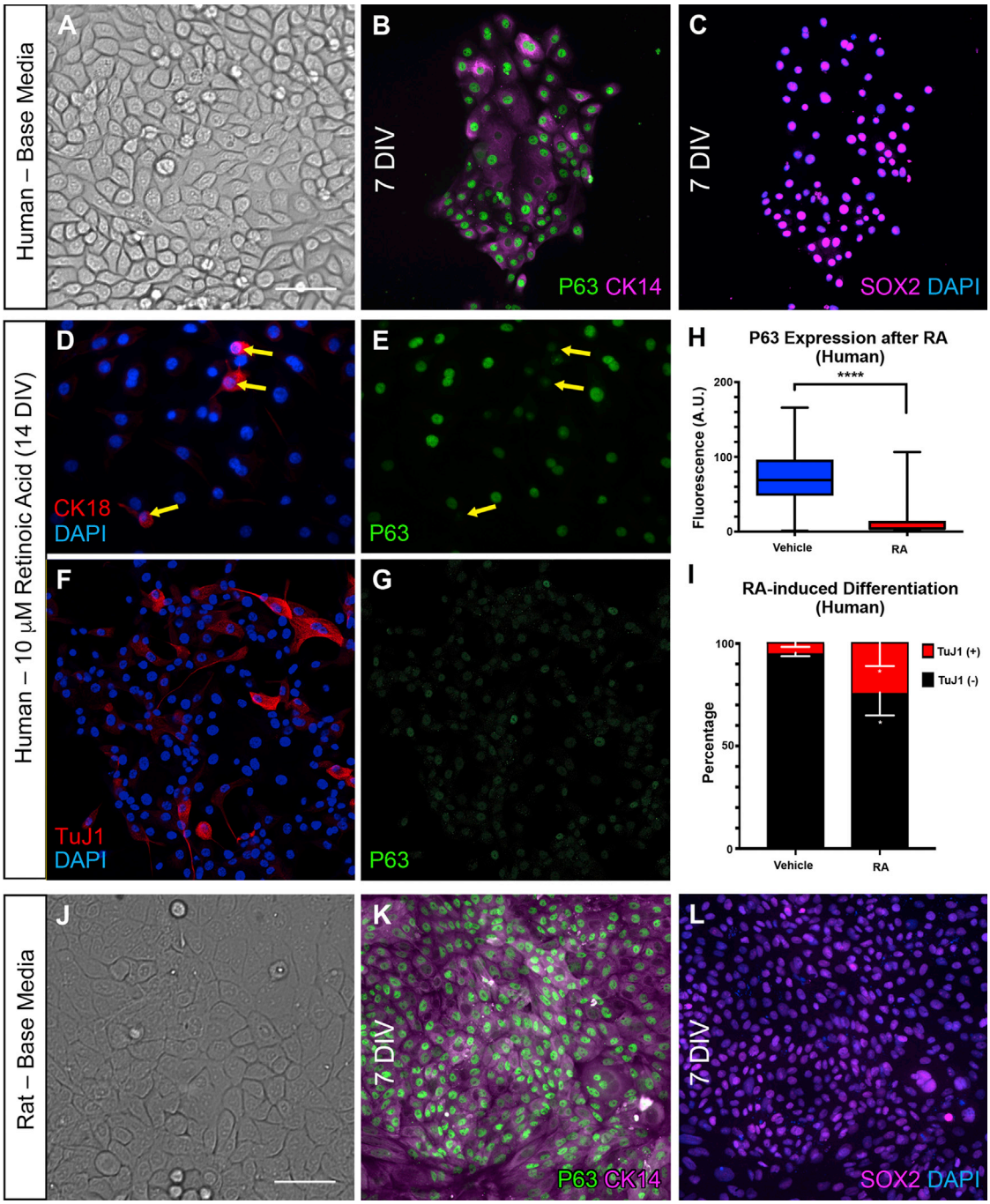

Figure 3. HBC Culture Protocol Supports Human and Rat HBC Growth

(A–C) HBC cultures from adult human biopsy grown for 7 days (A) express P63 (B), CK14 (B), and SOX2 (C).

(D–G) Human cultures show some differentiation after 14 days of 10 μM RA treatment. Scale bar in (A) represents 20 μm and applies to (B)–(G). (D and E) Photomicrographs of the same field. Differentiation into non-neuronal cells (D), exhibiting decreased P63 expression (E) (yellow arrows). (F and G) Photomicrographs of the same field. Differentiation into neurons cells (F), exhibiting decreased P63 expression (G).

(H) RA treatment of human HBCs produces a drop in P63 levels on a cell-by-cell basis as measured by fluorescence intensity after 3 days of treatment; box and whiskers plot, n = 3 independent wells for each condition, totaling 23,068 cells in the control and 2,265 after RA treatment. The t test compared the mean of the cell labeling values per replicate. ****$p < 0.0001$.

(legend continued on next page)

cells, such as the neuronal marker Tuj1 or the Sus/D/G marker CK18 (Figures 5C1-2 and 5D).

We also investigated whether retinoic acid (RA) could induce differentiation. RA knocks down P63 in other basal cell populations (Jean et al., 2011; Li et al., 2007; Yip and Tsao, 2008). It also fosters neuronal differentiation in the OE (Illing et al., 2002; Paschaki et al., 2013; Peluso et al., 2012). After 3 days of treatment with 10 μm RA, we observed expression of the Sus/D/G marker CK18 (Figure 5E1). By 7 days, Tuj1+ cells were present in the culture (Figure 5E2), while after 2 weeks of RA treatment both CK18+ and Tuj1+ cells were numerous and the complement of CK14+ cells was much reduced. Tuj1+ cells at this time point exhibited a bipolar morphology with long delicate processes similar to OSNs (Figure 5E3, inset). At the same 2-week time point, cultures grown without RA maintained CK14, expressed minimal CK18, and were Tuj1− (Figure 5F). When cultured in RA at the same dosage for 2 weeks, human HBCs *in vitro* also lost P63 expression (Figure 3) and began to stain with CK18 and Tuj1, although at a substantially lower frequency than mouse cultures, which may reflect generally slower differentiation of human cells.

Given that HBCs are known to give rise to RE *in vivo* (Xie et al., 2013), we also cultured HBCs to confluency under our modified PCX conditions followed by 2 weeks at the air-liquid interface in Pneumacult-ALI respiratory differentiation medium. We modified the manufacturer's protocol for growing RE by the substitution of laminin for a collagen substrate. After 2 weeks, CK14 and Tuj1 were absent from the cultures, and instead the cells exhibited broad expression of CK18 and a profoundly altered morphology (Figure 5G, inset), including the spiky cilia characteristic of an RE's brush border (Figure 5G, asterisks).

HBCs often differentiate into GBCs initially following activation *in vivo* (Leung et al., 2007; Fletcher et al., 2011; Schnittke et al., 2015; Fletcher et al., 2017; Gadye et al., 2017). Accordingly, we assayed RA-treated HBC cultures for markers of specific types of GBCs. Loss of P63 labeling was contemporaneous with expression of SEC8, which is a pan-GBC marker (Joiner et al., 2015), by a high percentage of the cells (Figures 4H, 4H′, and 5I). The SEC8+ cells were also marked by a reduced expression of CK14 (Figure 5I). SEC8-positivity and CK14-diminution were not observed in untreated cultures (Figure 5I′).

In addition to the cultures grown at the air-liquid interface depicted in Figures 5E–5G, differentiation was also observed in submerged cultures grown either on transwell membranes or on laminin-coated plastic (Figure 5J). It appears that cultures grown on plastic were less robust in their response to RA such that a greater fraction of cells remained CK14+ and a smaller fraction were labeled by CK18 and TuJ1 (Figure 5J). It is known that neural differentiation is markedly impacted by substrate stiffness (Discher et al., 2005), which may explain the difference observed here.

3D culture of the OE is thought to more closely recapitulate *in vivo* physiology compared with adherent culture (Jang et al., 2008; Krolewski et al., 2011). In parallel with previous demonstrations, passaged HBCs were embedded into growth factor-reduced Matrigel in the presence of RA, modifying a protocol developed for differentiating other epithelial cells (Drost et al., 2016). After 3 days, simple spheroidal structures appeared (Figure 5K1). We maintained these spheres for up to 7 days in the presence of RA (Figures 5K1–5K3). RA did not appear to affect sphere growth (Figures S1J–S1L). However, after 5 days of RA treatment, the spheres began to display decreased CK14 and increased SEC8 (Figures 5K–5M), suggesting initiation of differentiation through a GBC-like state. By 7 days, complex structures with tubular morphology were observed (Figure 5K3).

Cultured HBCs Contribute to Regeneration of Lesioned OE after Transplantation

Stem cell transplantation serves as the "gold standard" for assessing stem cell potency. HBCs cultured from Tam-treated *K5-CreER^{T2};fl(STOP)TdTomato* mice were infused intranasally into host adult mice lesioned by exposure to the olfactotoxic gas methyl bromide (MeBr), which prepares the host OE to accept engraftment (Chen et al., 2004; Goldstein et al., 1997; Jang et al., 2008; Lin et al., 2017; Schnittke et al., 2015) (Figure 6A). After 10 days, hosts were killed and the OE imaged. HBCs grown without RA did not engraft (0/12 host mice). However, cells treated with 10 μM RA for 7 days prior to transplantation did engraft (9/9 host mice) generating on the order of 100 clones per host animal. These were complex clones containing multiple cell types (Figures 6B1–6B3), including some PGP9.5+ neurons with apical processes (Figures 6C1–6C3), and CK18+ Sus cells (Figures 6D1–D3). In areas of the host OE in which enhanced severity of the lesion leads to respiratory metaplasia, culture-derived HBCs gave rise to CK18+ cells that also expressed βIV-Tubulin (Figures 6E1–6E3), an RE marker (Figures 5F1–5F3). This alternate

(I) RA treatment leads to significant increase in the percentage of Tuj1-stained cells; three independent wells. Mean ± SEM. Significance was determined using two-way ANOVA followed by Tukey's multiple comparison test. *$p < 0.05$.
(J–L) Cultures from rat OE express the HBC markers p63 and CK14 (K) and Sox2 (L) and expand more rapidly compared with human or mouse. Scale bar in (J) represents 20 μm and applies to (K)–(L).

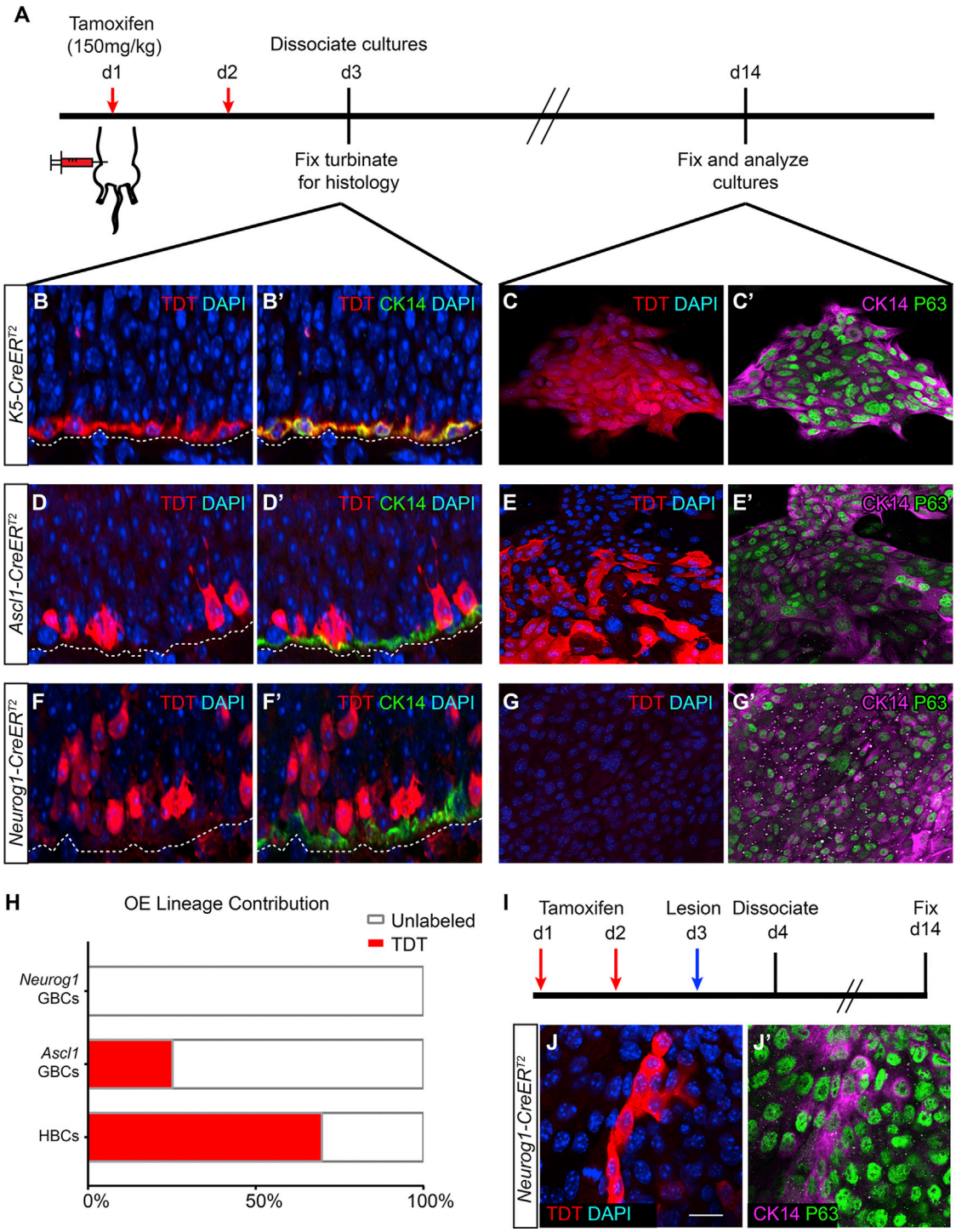

Figure 4. Genetic Recombination-Based Lineage Analysis Demonstrates that Cultured HBCs Are Derived from HBCs and GBCs *In Vivo*

(A) Experimental design and timeline.

(B–C′) Lineage trace using a *K5-CreER*^{T2} tamoxifen-dependent driver labels CK14+ HBCs with TDTOMATO (TDT) *in vivo* (B and B′) and gives rise to HBCs *in vitro* (C and C′).

(D–E′) Lineage trace using an *Ascl1-CreER*^{T2} tamoxifen-dependent driver labels ostensibly neuron-fated GBC progenitors apical to CK14+ HBCs *in vivo* (D and D′), but also labels HBCs in islands in mosaic distribution *in vitro* (E and E′).

(legend continued on next page)

result recapitulates the differentiation of the cultures in Pneumacult-ALI conditions where RE is the favored outcome (cf. Figures 5G and 6E1–6E3).

DISCUSSION

The results presented here establish a defined, tractable cell culture model for HBCs from mouse, rat, and human, which are the dormant, reserve stem cell population of the OE. The availability of cultured HBCs will facilitate studies of the mechanism(s) regulating their reserve status and their use for potential therapeutic purposes. The cultures maintain tissue-derived HBCs and support the transdifferentiation of selected GBC populations into HBCs, promote the differentiation of diverse olfactory and non-olfactory cell types following addition of RA, and promote cells that are capable of successful engraftment into host OE. Although HBCs are mitotically quiescent *in vivo*, the proliferation and expansion observed here in response to TGF-α echoes that of other reserve stem cells that have been grown in culture (Laumonier et al., 2017; Stange et al., 2013).

HBCs in culture closely resembled *in vivo* HBCs with respect to molecular phenotype and progenitor cell capacity after epithelial injury. At its extreme, the generation of ciliated, respiratory epithelial-like cells by olfactory HBCs *in vitro* and following engraftment into harshly lesioned OE mimics the respiratory metaplasia observed *in vivo* where HBCs also give rise to respirocytes following severe injury (Xie et al., 2013), and perhaps to the respiratory metaplasia that accompanies normal or artificially accelerated aging (Child et al., 2018; Holbrook et al., 2011). The culture system offers a novel tool for investigating the cues that toggle between regeneration of OE versus RE.

HBCs in culture can be activated either by excision of *p63* or by treatment with RA. Genetic excision *in vitro* mimics the activation of HBCs occasioned by epithelial injury *in vivo*. RA treatment of HBC cultures leads to the downregulation of P63 either directly or indirectly. The mechanism underlying activation *in vitro* is not known, although RA induces neuronal-like differentiation in immortalized OE-derived cell lines (Illing et al., 2002; Satoh and Takeuchi, 1995). Both the loss of CK14 and the increase in SEC8 in response to RA map to the transition from HBCs to GBCs. In the OE, HBC activation and that transition are restrained by Notch signaling, which drives *p63* expression *in vivo* (Herrick et al., 2017); HES1 expression by HBCs in culture prior to differentiation, are high, consistent with a similar role. Several reports indicate that RA and Notch signaling have an antagonistic relationship (Matulic et al., 2015; Mezquita et al., 2014; Ryu et al., 2015).

That the multiple epithelial types emerge in response of HBCs to RA suggests that manipulation of the culture environment will likely be useful for identifying potential mechanisms that drive cell-type-specific differentiation *in vivo* from activated HBCs (Schwob et al., 2017). With regard to neuronal differentiation following activation, previous reports have linked RA signaling and upregulation of ASCL1 expression (Bain et al., 1996; Jacob et al., 2013), which is required for GBC progression and olfactory neuronal differentiation (Cau et al., 1997).

Activation of the cultured HBCs is a prerequisite for their successful engraftment following transplantation. The failure of untreated HBC cultures to engraft fits with the failure of acutely isolated, dormant P63+ HBCs to engraft following animal-to-animal transplantation (Schnittke et al., 2015). Moreover, mitotic status is apparently irrelevant to the effectiveness of HBC engraftment, since proliferating, unactivated, cultured HBCs are equally as bad at engraftment as quiescent, dormant, *in vivo* HBCs.

While cultured HBCs engrafted into lesioned animals after activation, the fraction of neuronal progeny was lower than the proportion of cells evincing neuronal differentiation *in vitro* following RA treatment. As a consequence, the manipulation of the culture conditions with an eye toward enhancing neuronal differentiation after transplantation is a potentially powerful means of investigating the controls on neuronal differentiation. For example, enhanced neuronal differentiation following transplantation follows from maintaining 3D cultures of GBCs in medium that has been conditioned by a cell line derived from the lamina propria deep to the OE (Krolewski et al., 2011). Likewise, Wnt signaling seems to bias activated HBCs toward a neuronal fate, while not having an influence on activation per se (Fletcher et al., 2017).

In summary, we have developed a novel primary culture protocol for maintaining OE HBCs, a dormant reserve stem cell, *in vitro*. Our culture model provides a tool for investigating basic HBC behavior and analyzing

(F–G″) Lineage trace using a *Neurog1-CreER*^{T2} tamoxifen-dependent driver labels GBCs that function as immediate neuronal precursors *in vivo* (F and F′), but does not give rise to HBCs *in vitro* when isolated from uninjured OE (G and G′).

(H) Relative contributions of each lineage trace to cultures. Each count presents the ratio of TdTomato+ cells/total, n = 4 independent wells comprising over 600 cells/well for each type of lineage-traced progenitor (mean ± SEM).

(I) Experimental timeline for assessing the potency of *Neurog1*-expressing GBCs for the generation of HBCs *in vitro* when isolated from methimazole-lesioned OE.

(J and J′) After methimazole lesion, *Neurog1*-expressing GBCs *in vivo* did give rise on rare occasion to a few HBCs *in vitro*. Scale bar, 20 μm.

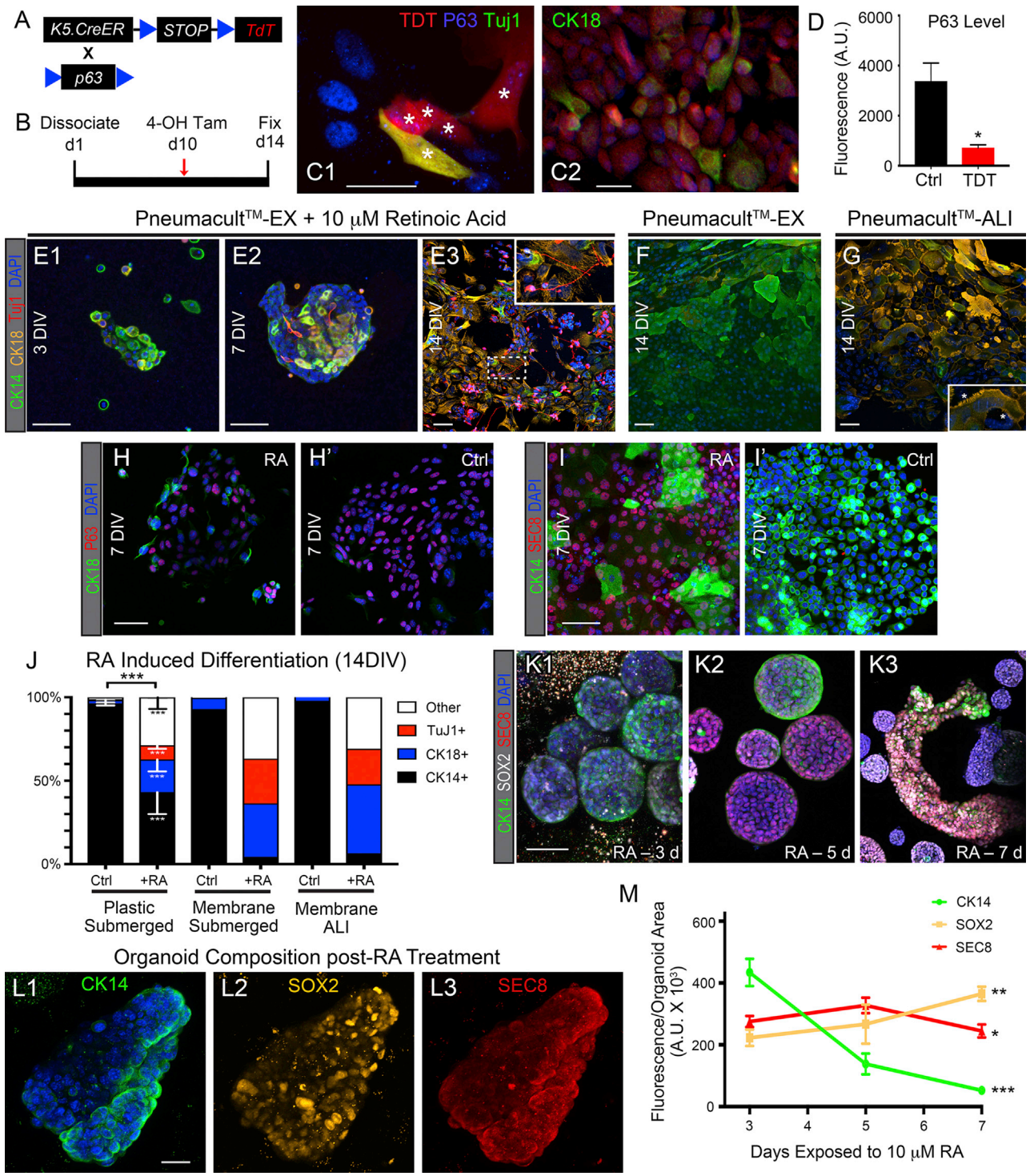

Figure 5. Cultured HBCs Maintain Potency and Give Rise to Diverse Olfactory Epithelial Cell Types *In Vitro*

(A) Schematic of the experimental strategy for excising *p63 in vitro* from HBCs harvested from *K5-CreER^{T2};p63$^{fl/fl}$;R26R-fl(stop)TdTomato* mice.

(B) Timeline for conditional excision of *p63*.

(C1 and C2) Cells that have recombined have low-to-undetectable levels of immunoreactive P63 and begin to stain with Tuj1, a neuronal marker (asterisks in C1), or CK18, a Sus cell marker (C2) by 4 days after tamoxifen.

(legend continued on next page)

their contribution to OE regeneration. The technique also supports human HBC expansion, providing a starting point for developing stem cell therapies based on autologous transplantation or pharmacologic activation of a patient's own dormant stem cells *in situ*.

EXPERIMENTAL PROCEDURES

Transgenic Animals and Breeding

All animals were maintained on *ad libitum* rodent chow and water and housed in a climate-controlled AALAC-accredited vivarium operating under a 12-h light/dark cycle. All protocols for the use of vertebrate animals are approved by the Committee for the Human Use of Animals at Tufts University School of Medicine. Eight-week old F1 mice were bred from C57/B6J and 129S1/Sv1MJ mice in house or were purchased from Jackson Laboratories (stock 101043). Adult male Sprague-Dawley rats were purchased from Taconic Biosciences (stock SD-M). *Ascl1-CreER^{T2}* mice (stock 012882), and the Cre reporter strain *R26R(TdTomato)* (stock 007909), constitutive GFP *Tg(UBC-GFP)* (stock 004353), and germline constitutive *Tg(Sox2-Cre)* (stock 004893) were purchased from Jackson Laboratories. *K5-CreER^{T2}* mice, *Neurog1-CreER^{T2}* mice, *p63$^{fl/fl}$* mice, and *ΔOMP-eGFP* mice have been described elsewhere and were generously provided by P. Chambon via R. Reed (Indra et al., 1999), L. Goodrich (Kim et al., 2011), A. Mills (Mills et al., 2002), and P. Mombaerts (Potter et al., 2001), respectively. Pancellular-TdT mice were generated in house by breeding *R26R(TdT)* mice to *Tg(Sox2-Cre)* mice.

Human Biopsy

Deidentified human OE and RE were obtained from the superior turbinate during routine sinus surgery for chronic sinusitis under a protocol approved by the Human Subjects Research Committee at Massachusetts Eye and Ear Infirmary. The tissue was immediately placed in culture medium and transferred to the laboratory on ice where further processing was performed.

Cell Culture

For rodent cultures, olfactory mucosa was isolated from nasal septum as illustrated in Figure 1. Tissue was minced in 2.7 mL of Pneumacult-Ex medium (STEMCELL Technologies [SCTech] 05008) or BEGM (Lonza CC-3170) containing 1× Gem21 NeuroPlex without vitamin A (Gemini Bio 400-161) and 1× N2 NeuroPlex (Gemini Bio 400-163) serum-free supplements in a 10-cm culture dish. Then, 300 μL of 10× collagenase/hyaluronidase cocktail was added, and samples were transferred to 15 mL conical centrifuge tubes, briefly vortexed and rotated at 37°C for 1 h. Samples were centrifuged at 80 × *g* for 30 s and supernatant aspirated. Pellets were triturated in 5 mL of pre-warmed 0.25% TrypLE for 2 min followed by addition of 10 mL of ice-cold Hank's balanced salt solution (HBSS) without calcium or magnesium and 15 μL of 1,000× trypsin inhibitor to prevent cell death. Samples were centrifuged for 5 min at 350 × *g*, resuspended in 1 mL of pre-warmed dispase and 50 μL of DNase 1 and briefly triturated for 2 min. Then, 10 mL of ice-cold HBSS and 11 μL of trypsin inhibitor were added and samples were filtered through Falcon 40 μm cell strainers into 50 mL conical centrifuge tubes. Samples were centrifuged for 5 min at 350 × *g*, supernatant aspirated, and pellet resuspended in complete HBC medium,

(D) Quantification of P63 fluorescence intensity 4 days after tamoxifen treatment (mean ± SEM), which is significantly reduced as assessed by Student's t test (n = 25). *p < 0.05.

(E1–G) Air-liquid interface (ALI) cultures at the indicated times after treatment with RA or media switch. (E1–E3) Following addition of RA, HBCs begin to express neuronal (inset in E3) and non-neuronal markers and undergo morphological differentiation that is well advanced after 14 days. (F) Cells grown without RA maintain CK14 expression through 2 weeks when cultured at an ALI. (G) OE cells grown in Pneumacult-ALI medium (devised for cultures of RE) express CK18 and display profound morphological changes including distinct respiratory brush borders (inset, asterisks).

(H and H′) P63 expression is reduced during RA-induced differentiation.

(I and I′) Cells treated with RA markedly increase expression of GBC marker SEC8. SEC8 expression is low to undetectable in CK14+ cells compared with neighboring CK14− cells.

(J) Quantification of the extent and type of differentiation after 2 weeks of RA induction. For cultures submerged on laminin-coated plastic, n = 4 independent wells (mean ± SEM). ANOVA with Tukey's multiple comparisons indicates a significant overall effect as well as significant differences when comparing composition with respect to each of the various marker-defined cell types. ***p < 0.001. A similar effect is observed for cells cultured on the upper side of the membrane of culture inserts whether submerged in medium or positioned at the ALI. In the latter two culture settings, n = 2 low power fields encompassing 500+ cells per field per well.

(K1–K3) 3D Matrigel-embedded cultures were established from passaged cultured HBCs and maintained in the presence of RA for 3, 5, or 7 days, respectively. Between 3 (K1) and 5 days (K2) of RA treatment, spheroid cultures develop histological heterogeneity and include cells that express the GBC marker Sec8, some of which also express a second GBC marker SOX2. Other cells that retain some measure of HBC differentiation are concentrated near the periphery of the spheres. (K3) By 7 days, complex tubular structures are present in the cultures and display discrete histological patterns. Z-projections with standard deviation intensity. Scale bar, 20 μm.

(L1–L3) Representative example of an organoid assayed for composition with the indicated markers. Overall fluorescent intensity was used as the measure of cellular composition.

(M) Assessment of organoid differentiation in response to RA at the durations of incubation indicated. Overall intensity of staining of the organoid with the three markers normalized to organoid area in the confocal projection; n = 16 organoids per time point (mean ± SEM). ANOVA analysis demonstrates significant shift in composition for each marker over time (CK14, SOX2, Kruskal-Wallis; SEC8, Shapiro-Wilk). *p < 0.05, **p < 0.01, ***p < 0.001.

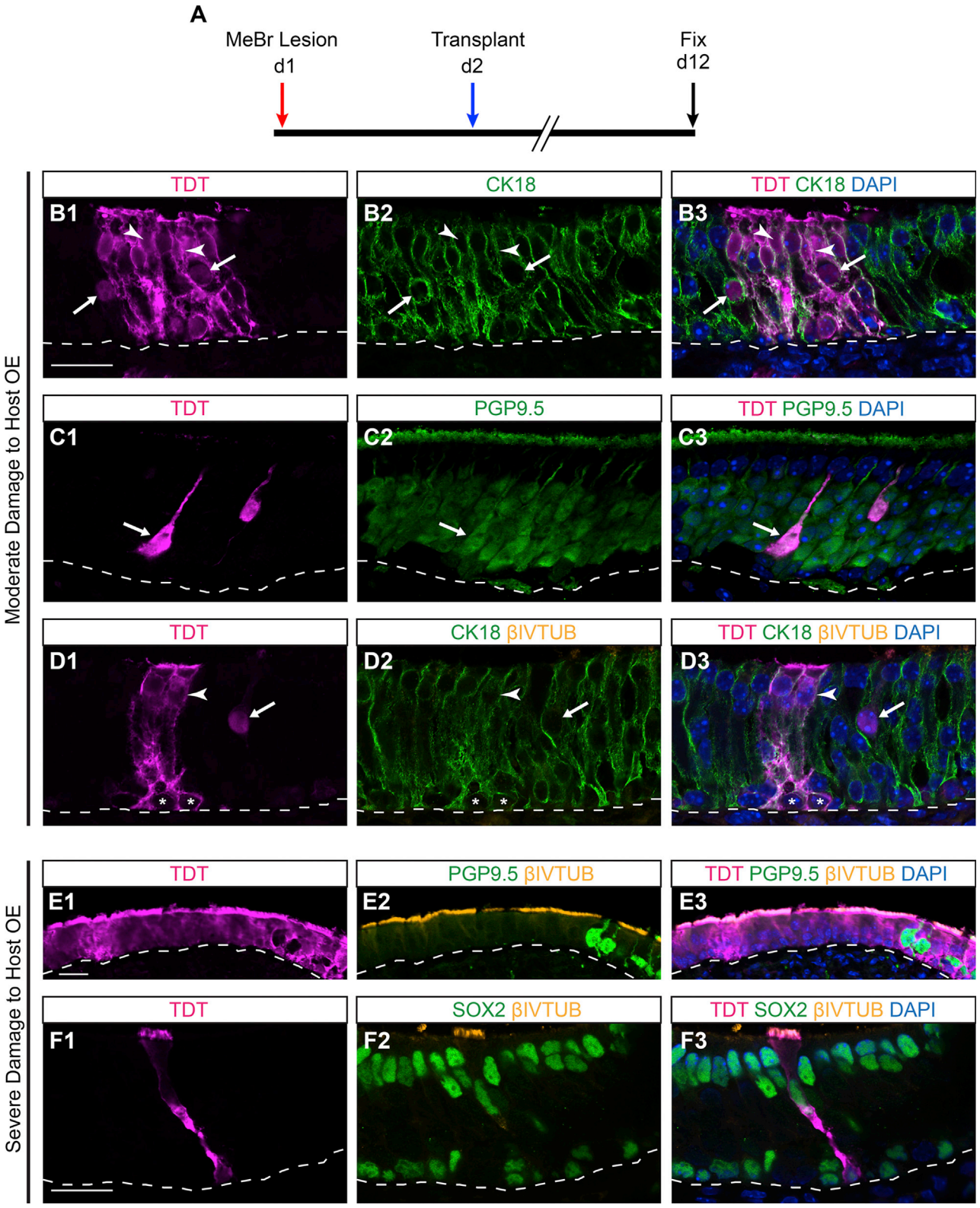

(legend on next page)

composed of Pneumacult-Ex medium containing 1× Glutamax, 1× Gem21 NeuroPlex without vitamin A, 1× N2 NeuroPlex, 10 μM Y27632 (Reagents Direct 53-B85), 200 pM recombinant TGF-α (R&D Systems 239-A-100), 1 μM A-83-01 (Tocris 2939), and 1 μM DMH-1 (Tocris 4126). Cells were then plated onto poly-D-lysine/laminin- coated plates or chamber slides (Corning). Cultures were fed with complete HBC medium every 2 days, although after the first change Y27632 was omitted. One mouse septum (bilateral dissection) was dissociated per 1.9 cm^2 growth area. For passaging, cells were detached with Accutase (SCTech 07,920) for 10 min at room temperature. Cells were frozen in complete medium containing 10% DMSO at −80°C overnight followed by storage in liquid nitrogen. Cells were replated after passaging or thawing into complete HBC medium with 20 μM Y27632. To induce differentiation, all-*trans*-RA was added to a final concentration of 10 μM and maintained until fixation.

Air-Liquid Interface Cultures and Sphere Cultures

For air-liquid interface (ALI) cultures, cells were passaged onto transwell membrane inserts (Corning CLS3396) coated with laminin and maintained for 4 days until islands were apparent, at which point the medium in the apical compartment was aspirated and remained absent for the rest of the culture. Pneumacult-ALI differentiation was conducted as directed by the manufacturer's protocol (SCTech). For sphere cultures, 20,000 post-passage HBCs were embedded in 40 μL of growth factor-reduced Matrigel and plated at the center of each well in a 24-well plate as previously described (Drost et al., 2016). For immunofluorescence, spheres were released from Matrigel by application of dispase for 30 min at room temperature followed by gentle agitation and resuspension in ice-cold PBS. Spheres were then transferred to an Eppendorf tube, spun at 60 × *g* for 5 min and resuspended in 4% paraformaldehyde (PFA) for fixation.

Lineage Trace

In vitro, (Z)-4-hydroxytamoxifen (Sigma H7904) was dissolved in DMSO and added to medium at a final concentration of 0.02 mg/mL. *In vivo*, tamoxifen was diluted in corn oil and used as previously described (Lin et al., 2017). All mice and rats were sacrificed by CO_2 exposure in accordance with Tufts DLAM regulations, sprayed with 70% ethanol, and dissected in an isolation hood.

Immunohistochemistry/Immunocytochemistry

For *in vitro* experiments, cells were fixed with 4% PFA in PBS (pH 7.5) for 15 min, followed by washing in PBS and a 10-min permeabilization in ice-cold methanol. Cells were then immunostained according to established protocols (Schnittke et al., 2015) (Table S1).

Proliferation Assay

Ethynyl deoxyuridine (EdU) was dissolved in DMSO and added to the medium at a final concentration of 20 μM. Cells were fixed after 1 h, and EdU detection was performed by the Click-IT EdU Alexa Fluor kit from Thermo Fisher (C10337).

Transcriptomic Analysis

RNA was harvested using the Zymo Research Quick-RNA MicroPrep kit (catalog no. R1050), following the manufacturer's instructions with the additional DNase treatment included. cDNA was generated using the NuGEN Ovation V2 kit (catalog no. 7102), prior to paired end, 100 base-pair sequencing using an Illumina HiSeq 2500 at a read depth of approximately 100 million reads per sample. Raw reads were processed using standard Tuxedo suite tools to the MM9 mouse transcriptomes build (Fletcher et al., 2017; Herrick et al., 2017; Kim et al., 2013; Lin et al., 2017). To pool bulk and single-cell RNA-seq, data were normalized by downsampling bulk data to the average depth of single-cell RNA-seq data and averaged across iterations. We found that downsampling the total number of transcripts to single-cell level complexities (3,500 genes) yielded data that exhibited no batch effect (across two single-cell RNA-seq datasets) and led to convergence of bulk and single-cell RNA-seq datasets. t-Distributed stochastic neighbor embedding (t-SNE) plots were used for dimension reduction and generated in R (Van der Maaten, 2014). Gene ontology was performed using QIAGEN's Ingenuity Pathway Analysis (QIAGEN, Redwood City).

Figure 6. Following Transplantation, Retinoic Acid-Treated HBCs Engraft and Generate Differentiated Epithelial Cell Types during Regeneration of the MeBr-Lesioned OE

(A) Experimental timeline for the procedure used to transplant the cultured, RA-treated HBCs by intranasal infusion.

(B1–B3) Coronal sections of post-lesion/post-transplant host OE in areas of the epithelium that have reconstituted as olfactory following moderate damage by MeBr exposure. OSNs (arrows), Sus cells (arrowheads), and basal cells (asterisks) were identified by morphology and marker expression. In areas of the epithelium that regenerate back into OE, RA-treated transplanted HBCs gave rise to complex clones containing multiple cell types.

(C1–C3) Other clones consisted of sparse PGP9.5 + neurons with intricate processes that ascend apically.

(D1–D3) In still others CK18+/βIV-TUBULIN- Sus cells and basal cell types were prominent; βIV-TUBULIN is a marker of ciliated respirocytes.

(E1–E3) In severely damaged areas where reconstitution of the epithelium as olfactory was impaired, engrafted cells gave rise to aneuronal ciliated columnar epithelial cells that expressed βIV-TUBULIN at their apical surface.

(F1–F3) Higher magnification of single graft-derived ciliated respirocytes embedded among Sus cells; the contribution of *in situ* HBCs to respiratory metaplasia has been described previously (Xie et al., 2013) as has the emergence of respirocytes following basal cell transplantation (Chen et al., 2004).

In all images, dashed lines indicate basal laminae. Scale bars, 20 μm.

Methyl Bromide and Methimazole Lesions

MeBr lesions were performed as previously described (Schnittke et al., 2015; Herrick et al., 2017). Briefly, 8-week-old male C57/B6 × 129 mice were passively exposed to MeBr gas at 180 ppm in pure air for 8 h and used as transplant hosts. *Neurog1* lineage trace mice (Figure 3) were lesioned via intraperitoneal injection of 75 mg/kg methimazole (Genter et al., 1995).

Transplantation

Transplantation was performed as previously described 24 h after MeBr exposure (Schnittke et al., 2015). Animals were euthanized 10 days later.

Tissue Processing

Tissue fixation, harvest, processing, and sectioning followed standard laboratory protocols using 1% periodate-lysine-paraformaldehyde fixative (Herrick et al., 2017).

Intracellular FACS Analysis of P63 and CK5

To isolate HBCs *ex vivo*, the OE was dissociated as previously described (Schnittke et al., 2015). *In vitro* HBCs were grown to confluency in 6-well plates. Cell medium was removed and replaced with warm Accutase to detach cells. The suspension was fixed and permeabilized utilizing the FIX & PERM Cell Permeabilization Kit (Thermo Fisher, GAS003) as described (Schnittke et al., 2015). After staining, cells were resuspended 1× HBSS and subjected to analytic flow cytometry analysis on the Becton-Dickinson LSRII. Boolean gating to remove debris, doublets, and select Hoechst 33,343+ cells was performed with Cytobank, and gated cells were visualized with R Studio (ggplot).

Imaging, Image Quantification, and Statistical Analysis

Cells and tissues were imaged on a Zeiss LSM800 confocal microscope or a Nikon 800E epifluorescence microscope. Images were processed using Fiji software to adjust color palette, balance, and contrast; all changes were applied to the entire image. Fluorescence quantification and image segmentation were performed using CellProfiler (Carpenter et al., 2006). P63 fluorescence was quantified in ImageJ by creating a DAPI mask, applying it to the P63 channel, and measuring the fluorescence of individual cells. Data were exported and analyzed in Prism 6. Further image analysis including 3D stack reconstruction was conducted using Icy platform (de Chaumont et al., 2012). Student's t test was used to compare values with normal distributions. One- or two-way ANOVA with Tukey's method was used for multiple mean comparisons. For all statistical analyses, the number of animals or culture wells are noted in the figure legends. In all graphs, *$p < 0.05$, **$p < 0.01$, ***$p < 0.001$, ****$p < 0.0001$. Error bars represent the standard error of the mean.

ACCESSION NUMBERS

Data generated herein are deposited at GEO: GSE103577. Additional RNA-seq data were accessed from GEO: GSE95601, GSE92842, GSE92779 (Fletcher et al., 2017).

SUPPLEMENTAL INFORMATION

Supplemental Information can be found online at https://doi.org/10.1016/j.stemcr.2019.02.014.

AUTHOR CONTRIBUTIONS

J.P., B.L., C.M.B.-C., D.B.H., and J.E.S. designed the research; J.P., B.L., C.M.B.-C., D.B.H., and W.J. performed the research; B.L., E.H.H., and J.H.C. contributed new reagents/analytic tools; J.P., B.L., C.M.B.-C., D.B.H., and J.E.S. analyzed data; and J.P., B.L., C.M.B.-C., and J.E.S. wrote the paper.

ACKNOWLEDGMENTS

The authors thank Po Kwok-Tse for her outstanding technical assistance. Funded by the NIH, USA: R01 DC002167 (J.E.S.), F31 DC014637 (B.L.), F30 DC013962 (D.B.H.), and F31 DC014398 (J.H.C.).

Received: October 20, 2017
Revised: February 27, 2019
Accepted: February 28, 2019
Published: March 28, 2019

REFERENCES

Bain, G., Ray, W.J., Yao, M., and Gottlieb, D.I. (1996). Retinoic acid promotes neural and represses mesodermal gene expression in mouse embryonic stem cells in culture. Biochem. Biophys. Res. Commun. *223*, 691–694.

Beites, C., Kawauchi, S., Crocker, C., and Calof, A. (2005). Identification and molecular regulation of neural stem cells in the olfactory epithelium. Exp. Cell Res. *306*, 309–316.

Carpenter, A.E., Jones, T.R., Lamprecht, M.R., Clarke, C., Kang, I.H., Friman, O., Guertin, D.A., Chang, J.H., Lindquist, R.A., Moffat, J., et al. (2006). CellProfiler: image analysis software for identifying and quantifying cell phenotypes. Genome Biol. *7*, R100.

Cau, E., Gradwohl, G., Fode, C., and Guillemot, F. (1997). Mash1 activates a cascade of bHLH regulators in olfactory neuron progenitors. Development *124*, 1611–1621.

de Chaumont, F., Dallongeville, S., Chenouard, N., Hervé, N., Pop, S., Provoost, T., Meas-Yedid, V., Pankajakshan, P., Lecomte, T., Le Montagner, Y., et al. (2012). Icy: an open bioimage informatics platform for extended reproducible research. Nat. Methods *9*, 690–696.

Chen, X., Fang, H., and Schwob, J. (2004). Multipotency of purified, transplanted globose basal cells in olfactory epithelium. J. Comp. Neurol. *469*, 457–474.

Child, K.M., Herrick, D.B., Schwob, J.E., Holbrook, E.H., and Jang, W. (2018). The neuroregenerative capacity of olfactory stem cells is not limitless: implications for aging. J. Neurosci. *38*, 6806–6824.

Van Der Maaten, L. (2014). Accelerating t-SNE using tree-based algorithms. J. Mach. Learn. Res. *15*, 3221–3245.

Discher, D.E., Janmey, P., and Wang, Y.L. (2005). Tissue cells feel and respond to the stiffness of their substrate. Science *310*, 1139–1143.

Drost, J., Karthaus, W.R., Gao, D., Driehuis, E., Sawyers, C.L., Chen, Y., and Clevers, H. (2016). Organoid culture systems for prostate epithelial and cancer tissue. Nat. Protoc. *11*, 347–358.

Farbman, A.I., and Buchholz, J.A. (1996). Transforming growth factor-alpha and other growth factors stimulate cell division in olfactory epithelium in vitro. J. Neurobiol. *30*, 267–280.

Farbman, A.I., and Ezeh, P.I. (2000). TGF-alpha and olfactory marker protein enhance mitosis in rat olfactory epithelium in vivo. Neuroreport *11*, 3655–3658.

Fletcher, R.B., Prasol, M.S., Estrada, J., Baudhuin, A., Vranizan, K., Choi, Y.G., and Ngai, J. (2011). P63 regulates olfactory stem cell self-renewal and differentiation. Neuron *72*, 748–759.

Fletcher, R.B., Das, D., Gadye, L., Street, K.N., Baudhuin, A., Wagner, A., Cole, M.B., Flores, Q., Choi, Y.G., Yosef, N., et al. (2017). Deconstructing olfactory stem cell trajectories at single-cell resolution. Cell Stem Cell *20*, 817–830.

Gadye, L., Das, D., Sanchez, M.A., Street, K., Baudhuin, A., Wagner, A., Cole, M.B., Choi, Y.G., Yosef, N., Purdom, E., et al. (2017). Injury activates transient olfactory stem cell states with diverse lineage capacities. Cell Stem Cell *21*, 775–790.

Genter, M.B., Deamer, N.J., Blake, B.L., Wesley, D.S., and Levi, P.E. (1995). Olfactory toxicity of methimazole: dose-response and structure-activity studies and characterization of flavin-containing monooxygenase activity in the Long-Evans rat olfactory mucosa. Toxicol. Pathol. *23*, 477–486.

Getchell, T.V., Narla, R.K., Little, S., Hyde, J.F., and Getchell, M.L. (2000). Horizontal basal cell proliferation in the olfactory epithelium of transforming growth factor-alpha transgenic mice. Cell Tissue Res. *299*, 185–192.

Goldstein, B.J., Fang, H., and Schwob, J.E. (1997). Transplantation of multipotent progenitors from the adult olfactory epithelium. Neuroreport *9*, 1611–1617.

Goldstein, B.J., Fang, H., Youngentob, S.L., and Schwob, J.E. (1998). Transplantation of multipotent progenitors from the adult olfactory epithelium. Neuroreport *9*, 1611–1617.

Goldstein, B.J., Goss, G.M., Hatzistergos, K.E., Rangel, E.B., Seidler, B., Saur, D., and Hare, J.M. (2015). Adult c-Kit(+) progenitor cells are necessary for maintenance and regeneration of olfactory neurons. J. Comp. Neurol. *523*, 15–31.

Herrick, D.B., Lin, B., Peterson, J., Schnittke, N., and Schwob, J.E. (2017). Notch1 maintains dormancy of olfactory horizontal basal cells, a reserve neural stem cell. Proc. Natl. Acad. Sci. U S A *114*, E5589–E5598.

Holbrook, E., Szumowski, K., and Schwob, J. (1995). An immunochemical, ultrastructural, and developmental characterization of the horizontal basal cells of rat olfactory epithelium. J. Comp. Neurol. *363*, 129–146.

Holbrook, E.H., Wu, E., Curry, W.T., Lin, D.T., and Schwob, J.E. (2011). Immunohistochemical characterization of human olfactory tissue. Laryngoscope *121*, 1687–1701.

Illing, N., Boolay, S., Siwoski, J.S., Casper, D., Lucero, M.T., and Roskams, A.J. (2002). Conditionally immortalized clonal cell lines from the mouse olfactory placode differentiate into olfactory receptor neurons. Mol. Cell. Neurosci. *20*, 225–243.

Indra, A.K., Warot, X., Brocard, J., Bornert, J.M., Xiao, J.H., Chambon, P., and Metzger, D. (1999). Temporally-controlled site-specific mutagenesis in the basal layer of the epidermis: comparison of the recombinase activity of the tamoxifen-inducible Cre-ER(T) and Cre-ER(T2) recombinases. Nucleic Acids Res. *27*, 4324–4327.

Jacob, J., Kong, J., Moore, S., Milton, C., Sasai, N., Gonzalez-Quevedo, R., Terriente, J., Imayoshi, I., Kageyama, R., Wilkinson, D.G., et al. (2013). Retinoid acid specifies neuronal identity through graded expression of Ascl1. Curr. Biol. *23*, 412–418.

Jang, W., Lambropoulos, J., Woo, J.K., Peluso, C.E., and Schwob, J.E. (2008). Maintaining epitheliopoietic potency when culturing olfactory progenitors. Exp. Neurol. *214*, 25–36.

Jean, J., Soucy, J., and Pouliot, R. (2011). Effects of retinoic acid on keratinocyte proliferation and differentiation in a psoriatic skin model. Tissue Eng. Part A *17*, 1859–1868.

Joiner, A., Green, W., McIntyre, J., Allen, B., Schwob, J., and Martens, J. (2015). Primary cilia on horizontal basal cells regulate regeneration of the olfactory epithelium. J. Neurosci. *35*, 13761–13772.

Kim, E.J., Hori, K., Wyckoff, A., Dickel, L.K., Koundakjian, E.J., Goodrich, L.V., and Johnson, J.E. (2011). Spatiotemporal fate map of neurogenin1 (Neurog1) lineages in the mouse central nervous system. J. Comp. Neurol. *519*, 1355–1370.

Kim, D., Pertea, G., Trapnell, C., Pimentel, H., Kelley, R., and Salzberg, S.L. (2013). TopHat2: accurate alignment of transcriptomes in the presence of insertions, deletions and gene fusions. Genome Biol. *14*, R36.

Krolewski, R.C., Jang, W., and Schwob, J.E. (2011). The generation of olfactory epithelial neurospheres in vitro predicts engraftment capacity following transplantation in vivo. Exp. Neurol. *229*, 308–323.

Laumonier, T., Bermont, F., Hoffmeyer, P., Kindler, V., and Menetrey, J. (2017). Human myogenic reserve cells are quiescent stem cells that contribute to muscle regeneration after intramuscular transplantation in immunodeficient mice. Sci. Rep. *7*, 3462.

Leung, C.T., Coulombe, P.A., and Reed, R.R. (2007). Contribution of olfactory neural stem cells to tissue maintenance and regeneration. Nat. Neurosci. *10*, 720–726.

Li, H., Cherukuri, P., Li, N., Cowling, V., Spinella, M., Cole, M., Godwin, A.K., Wells, W., and Direnzo, J. (2007). Nestin is expressed in the basal/myoepithelial layer of the mammary gland and is a selective marker of basal epithelial breast tumors. Cancer Res. *67*, 501–510.

Lin, B., Coleman, J.H., Peterson, J.N., Zunitch, M.J., Jang, W., Herrick, D.B., and Schwob, J.E. (2017). Injury induces endogenous reprogramming and dedifferentiation of neuronal progenitors to multipotency. Cell Stem Cell *21*, 761–774.

Matulic, M., Skelin, J., Radic-Kristo, D., Kardum-Skelin, I., Grcevic, D., and Antica, M. (2015). Notch affects the prodifferentiating effect of retinoic acid and PMA on leukemic cells. Cytometry A *87*, 129–136.

Mezquita, B., Mezquita, J., Barrot, C., Carvajal, S., Pau, M., Mezquita, P., and Mezquita, C. (2014). A truncated-flt1 isoform of breast cancer cells is upregulated by notch and downregulated by retinoic acid. J. Cell. Biochem. *115*, 52–61.

Mills, A.A., Qi, Y., and Bradley, A. (2002). Conditional inactivation of p63 by Cre-mediated excision. Genesis *32*, 138–141.

Monti Graziadei, G.A., and Graziadei, P.P.C. (1979). Neurogenesis and neuron regeneration in the olfactory system of mammals. II. Degeneration and reconstitution of the olfactory sensory neurons after axotomy. J. Neurocytol. *8*, 197–213.

Mou, H., Vinarsky, V., Tata, P., Brazauskas, K., Choi, S., Crooke, A., Zhang, B., Solomon, G., Turner, B., Bihler, H., et al. (2016). Dual SMAD signaling inhibition enables long-term expansion of diverse epithelial basal cells. Cell Stem Cell *19*, 217–231.

Murdoch, B., and Roskams, A.J. (2007). Olfactory epithelium progenitors: insights from transgenic mice and in vitro biology. J. Mol. Histol. *38*, 581–599.

Packard, A., Schnittke, N., Romano, R.-A., Sinha, S., and Schwob, J.E. (2011). DeltaNp63 regulates stem cell dynamics in the mammalian olfactory epithelium. J. Neurosci. *31*, 8748–8759.

Paschaki, M., Cammas, L., Muta, Y., Matsuoka, Y., Mak, S.-S., Rataj-Baniowska, M., Fraulob, V., Dollé, P., and Ladher, R.K. (2013). Retinoic acid regulates olfactory progenitor cell fate and differentiation. Neural Dev. *8*, 13.

Peluso, C., Jang, W., Dräger, U., and Schwob, J. (2012). Differential expression of components of the retinoic acid signaling pathway in the adult mouse olfactory epithelium. J. Comp. Neurol. *520*, 3707–3726.

Potter, S.M., Zheng, C., Koos, D.S., Feinstein, P., Fraser, S.E., and Mombaerts, P. (2001). Structure and emergence of specific olfactory glomeruli in the mouse. J. Neurosci. *21*, 9713–9723.

Ryu, J.H., Kong, H.J., Park, J.Y., Lim, K.E., An, C.M., Lee, J., and Yeo, S.Y. (2015). Generation of late-born neurons in the ventral spinal cord requires the coordination of retinoic acid and Notch signaling. Neurosci. Lett. *602*, 95–98.

Satoh, M., and Takeuchi, M. (1995). Induction of NCAM expression in mouse olfactory keratin-positive basal cells in vitro. Dev. Brain Res. *87*, 111–119.

Schnittke, N., Herrick, D.B., Lin, B., Peterson, J., Coleman, J.H., Packard, A.I., Jang, W., and Schwob, J.E. (2015). Transcription factor p63 controls the reserve status but not the stemness of horizontal basal cells in the olfactory epithelium. Proc. Natl. Acad. Sci. U S A *112*, E5068–E5077.

Schwob, J.E., Youngentob, S.L., and Mezza, R.C. (1995). Reconstitution of the rat olfactory epithelium after methyl bromide-induced lesion. J. Comp. Neurol. *412*, 439–457.

Schwob, J.E., Jang, W., Holbrook, E.H., Lin, B., Herrick, D.B., Peterson, J.N., and Hewitt Coleman, J. (2017). Stem and progenitor cells of the mammalian olfactory epithelium: taking poietic license. J. Comp. Neurol. *525*, 1034–1054.

Stange, D.E., Koo, B.K., Huch, M., Sibbel, G., Basak, O., Lyubimova, A., Kujala, P., Bartfeld, S., Koster, J., Geahlen, J.H., et al. (2013). Differentiated Troy+ chief cells act as reserve stem cells to generate all lineages of the stomach epithelium. Cell *155*, 357–368.

Xie, F., Fang, C., Schnittke, N., Schwob, J.E., and Ding, X. (2013). Mechanisms of permanent loss of olfactory receptor neurons induced by the herbicide 2,6-dichlorobenzonitrile: effects on stem cells and noninvolvement of acute induction of the inflammatory cytokine IL-6. Toxicol. Appl. Pharmacol. *272*, 598–607.

Yip, Y.L., and Tsao, G.S.W. (2008). Regulation of p63 expression in primary and immortalized nasopharyngeal epithelial cells. Int. J. Oncol. *33*, 713–724.